Progress of Theoretical Physics, Vol. 123, No. 6, June 2010

# Various Synchronization Phenomena in Discrete-Time Coupled Chaotic Rotors

Kai MORINO,[1,*)] Takehiko HORITA[2] and Syuji MIYAZAKI[1]

[1]*Department of Applied Analysis and Complex Dynamical Systems, Graduate School of Informatics, Kyoto University, Kyoto 606-8501, Japan*
[2]*Department of Mathematical Sciences, Osaka Prefecture University, Sakai 599-8531, Japan*

(Received March 5, 2010; Revised May 5, 2010)

Various synchronizations and related phenomena in discrete-time coupled chaotic rotors are studied. For unidirectional and bidirectional couplings, various dynamical forms of chaotic phase synchronization (CPS) and their relation to the Lyapunov spectra are shown. For a small positive maximum Lyapunov exponent of the coupled element in the case of the unidirectional coupling, the coupling strength at which CPS is achieved almost coincides with the coupling strength at which generalized synchronization (GS) is achieved. On the other hand, for a large positive maximum Lyapunov exponent, the coupling strength is much smaller on the CPS transition point than on the GS transition point. Statistical properties of the phase difference are analytically and numerically studied by large-deviation analysis. On the basis of the grand canonical formalism, the fluctuation spectrum is theoretically derived, which is compared with the numerical results. These agree with the theoretical estimation, and large deviations are detected out of the domain in which the central limit theorem cannot be applied.

Subject Index: 055

## §1. Introduction

Originating with Huygens' observation of coupled pendula, various synchronization phenomena have been studied, mainly by considering continuous-time dynamical systems.[1)] Introducing a suitable Poincaré surface, one can obtain a discrete-time dynamical system called a Poincaré map. Discrete-time models are also useful for analyzing large-deviation statistics,[2),3)] singularity spectra,[4)] and spectral densities[5)] of modulational intermittency, also known as on-off intermittency. This phenomenon occurs when complete synchronization, that is, synchronization between identical chaotic oscillators,[6),7)] is slightly broken.

Various synchronization phenomena exist between chaotic oscillators. For a chaotic dynamical system whose *phase* and *amplitude* can be defined, one can obtain phase-synchronized and amplitude-desynchronized states between chaotic oscillators in which control parameters are slightly different. This is called chaotic phase synchronization (CPS).[8)–12)]

For a unidirectionally coupled system consisting of a driving system and a response system, generalized synchronization (GS) is observed, in which state variables

*) Present address: Department of Mathematical Informatics, Graduate School of Information Science and Technology, University of Tokyo, Tokyo 113-8656, Japan.

of the response system are given by a function of those of the driving system.[13),14)]

Starting from an equation of motion of a harmonic oscillator with a periodic external kicking, Fujisaka et al.[15)] introduced the following map described with a phase $\psi$

$$\psi_{n+1} = e^{i\omega} f_a(\psi_n, \psi_n^*) \tag{1·1}$$

with

$$f_a(\psi, \psi^*) \equiv \psi_n + F_a(\psi, \psi^*), \tag{1·2}$$

where asterisks denote complex conjugates and the natural frequency of the harmonic oscillator is given by $\omega$. A specific choice of the function $f_a$ yields the Ikeda map in the field of quantum optics.[16)] We fix the function as

$$f_a(\psi, \psi^*) = (a - (1 + ib)|\psi|^2)\psi \tag{1·3}$$

in the following and define the amplitude $R$ and the phase $\theta$ as $R \equiv |\psi|$ and $\theta \equiv \arg(\psi)$, respectively. Note that, for the choice of Eq. (1·3), Eq. (1·1) possesses a Lyapunov exponent of zero owing to its invariance under the transformation $\psi \to e^{-i\varphi}\psi$.

In the same way, coupled equations of motion of a harmonic oscillator with a periodic external kicking yield the following coupled map:[15)]

$$\psi_{n+1}^{(j)} = e^{i\omega_j + \mathcal{D}} f_{a_j}(\psi_n^{(j)}, \psi_n^{(j)*}) \tag{1·4}$$

with the coupling operator $\mathcal{D}$. For a quantity $g_j$ concerning the $j$th oscillator, $D$ satisfies $\mathcal{D}g_j = \sum_k B_{jk} g_k$ with coefficients $B_{jk}$ and $e^{i\omega_j + \mathcal{D}} g_j = \sum_k (e^{\hat{\Lambda}})_{jk} g_k$ with the coupling matrix $\hat{\Lambda}$ given by $(\hat{\Lambda})_{jk} = i\omega_j \delta_{jk} + B_{jk}$, where $\delta_{jk}$ denotes Kronecker's delta.

In the following, we confine ourselves to a coupled system $(\psi_n^{(1)}, \psi_n^{(2)})$ consisting of two elements. The instantaneous phase difference $\Delta\theta_n$ is given by $\Delta\theta_n \equiv \theta_n^{(1)} - \theta_n^{(2)}$. We define the average frequency difference $\Delta\Omega$ as

$$\Delta\Omega \equiv \lim_{T\to\infty} (\Delta\theta_T - \Delta\theta_0)/T, \tag{1·5}$$

and we define the CPS as the state satisfying

$$\Delta\Omega = 0. \tag{1·6}$$

The average value of the phase difference $\Delta\theta_n$ obeys

$$\langle \Delta\theta_n \rangle = \Delta\theta_0 + \Delta\Omega \cdot n, \tag{1·7}$$

where $\langle \cdots \rangle$ is the statistical average over an ensemble.

We focus on the following points in this paper. It is easier to adjust a suitable parameter $a$ of the chaotic map given by Eqs. (1·1) – (1·3) to yield a desired value of the largest Lyapunov exponent, as shown in the following section. We obtain

the Lyaponov spectra for a coupled system consisting of undeveloped and developed chaotic elements with small and large values, respectively, of the largest Lyapunov exponent. Then, we perform a return map (RM) analysis for unidirectionally and bidirectionally coupled systems whose elements are weak or developed chaos. From the RM in the vicinity of the CPS transition point, where the CPS is slightly broken, we can assume a statistical property of the time interval of the phase slip. On the basis of this assumption, we derive large-deviation properties of the phase difference.

In §2, we perform RM analyses and study the parameter dependence and coupling strength dependence of the signs of Lyapunov exponents in the vicinity of the CPS transition for unidirectionally and bidirectionally coupled systems. The relative relationship between the CPS transition points and the position at which the Lyapunov exponents change sign on the plane spanned by the parameter $a$ and the coupling constant differs considerably between weakly and strongly chaotic elements. This is not the case for the bidirectional coupling. We apply a large-deviation analysis to the fluctuation of phase differences, when the CPS is slightly broken in §3. Our theoretical estimation agrees with the numerical results. The final section is devoted to concluding remarks.

## §2. Lyapunov spectra and various dynamical forms of the chaotic phase synchronization

In this section, we show various dynamical forms of the CPS and their relation to the Lyapunov spectra for unidirectional and bidirectional couplings. The relationship between the coupling strength at which the magnitude relation of the Lyapunov exponents changes and that at which the CPS occurs, the RMs $(\Delta\theta_n, \Delta\theta_{n+n_0})$ of the phase difference $\Delta\theta_n$, and the bifurcation diagrams, that is, the dependences of the amplitude on parameter $a$, are also analyzed. In the following, we set $\omega_1 = 0.11, \omega_2 = 0.03$, $\Delta\omega \equiv \omega_1 - \omega_2 = 0.08$, $a_1 = a_2 = a$, and $b = 0$. This setting always yields phase-coherent oscillations, different from phase-coherent or phase-incoherent Rössler oscillations.[10)]

For a single oscillator $\psi_n$ under the above parameter setting, the temporal evolution of the amplitude $R_n \equiv |\psi_n| \geq 0$ is independent of the phase dynamics $\theta_{n+1} = \theta_n + \omega$ and governed by the unimodal mapping $R_{n+1} = (a - R_n^2)R_n$ from the interval $I = [0, \sqrt{a}]$ into $I$, which takes a local maximum value at $R = \sqrt{a/3}$. The fixed point $R = 0$ always exists. The other fixed point $R = \sqrt{a-1}$ in $I$ exists for $a \geq 1$. The periodic points with period two $R = \sqrt{\frac{a \pm \sqrt{a^2-4}}{2}}$ in $I$ exist for $a \geq 2$. The bifurcation diagram of the amplitude against the parameter $a$ is shown in Fig. 1. At $a \simeq 2.314815$ and $a \simeq 2.36089376$, four chaotic bands merge into two bands and two bands merge into a single band, respectively. The attractor is destroyed at $a = 3\sqrt{3}/2 \simeq 2.598$, where the trajectory starting at $R_0 = \sqrt{a}/3$ takes the local maximum $R_1 = \sqrt{a}$, and then collides with the unstable fixed point $R_2 = 0$. One of the Lyapunov exponents is always zero, which originates from the marginal phase dynamics $\theta_{n+1} = \theta_n + \omega$. The sign of the other Lyapunov exponent is determined by the dynamics of $R_n$, which is controlled by the parameter $a$.

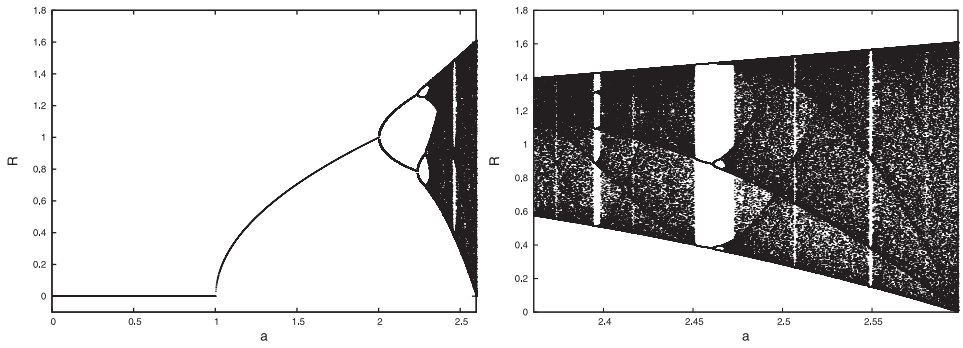


(a) (b)

Fig. 1. Bifurcation diagrams of the amplitude $R = |\psi|$ of the single oscillator $\psi$ plotted against the parameter $a$ for the whole parameter range $0 \leq a \leq 3\sqrt{3}/2$ in (a) and for the single-band range $2.361 \leq a \leq 3\sqrt{3}/2$ in (b). Chaotic bands and periodic windows are observed.

### 2.1. *Unidirectional coupling*

In the case of a unidirectional coupling from $\psi^{(1)}$ to $\psi^{(2)}$, the coupling term is given by $\mathcal{D}g_1 = 0$ and $\mathcal{D}g_2 = K(g_1 - g_2)$, and the coupling matrix $\hat{\Lambda}$ satisfies

$$\hat{\Lambda} = \begin{pmatrix} i\omega_1 & 0 \\ K & i\omega_2 - K \end{pmatrix}, \tag{2·1}$$

where $K$ is the coupling strength. For this setting, from Eq. (1·3) we have

$$\begin{cases} \psi_{n+1}^{(1)} & = e^{i\omega_1} f_{a_1}(\psi_n^{(1)}, \psi_n^{(1)*}), \\ \psi_{n+1}^{(2)} & = A(\Delta\omega)(1 - e^{-K - i\Delta\omega}) e^{i\omega_1} f_{a_1}(\psi_n^{(1)}, \psi_n^{(1)*}) + e^{-K} e^{i\omega_2} f_{a_2}(\psi_n^{(2)}, \psi_n^{(2)*}) \end{cases} \tag{2·2}$$

with $A(\Delta\omega) \equiv K(K - i\Delta\omega)/(K^2 + (\Delta\omega)^2)$. For $K \to \infty$, we have $\psi_{n+1}^{(2)} \to e^{i\omega_1} f_{a_1}(\psi_n^{(1)}, \psi_n^{(1)*}) = \psi_{n+1}^{(1)}$ i.e., two oscillators coincide with each other. One of the four Lyapunov exponents is always zero as a result of the marginal phase dynamics of the driving system $\psi_n^{(1)}$.

Defining $\hat{\psi}_n \equiv \psi_n \exp(-in\omega_1)$, we can rewrite Eq. (2·2) as

$$\begin{cases} \hat{\psi}_{n+1}^{(1)} & = f_{a_1}(\hat{\psi}_n^{(1)}, \hat{\psi}_n^{(1)*}), \\ \hat{\psi}_{n+1}^{(2)} & = A(\Delta\omega)(1 - e^{-K - i\Delta\omega}) f_{a_1}(\hat{\psi}_n^{(1)}, \hat{\psi}_n^{(1)*}) + e^{-K} e^{-i\Delta\omega} f_{a_2}(\hat{\psi}_n^{(2)}, \hat{\psi}_n^{(2)*}) \end{cases} \tag{2·3}$$

using the fact that $f_a \to e^{i\varphi} f_a$ holds for $\psi \to e^{i\varphi}\psi$ in Eq. (1·3). Since $f_a(\psi, \psi^*)^* = f_a(\psi^*, \psi)$ holds in Eq. (1·3) for $b = 0$, the complex conjugate of Eq. (2·3) yields

$$\begin{cases} \bar{\psi}_{n+1}^{(1)} & = f_{a_1}(\bar{\psi}_n^{(1)}, \bar{\psi}_n^{(1)*}), \\ \bar{\psi}_{n+1}^{(2)} & = A(-\Delta\omega)(1 - e^{-K + i\Delta\omega}) f_{a_1}(\bar{\psi}_n^{(1)}, \bar{\psi}_n^{(1)*}) + e^{-K} e^{i\Delta\omega} f_{a_2}(\bar{\psi}_n^{(2)}, \bar{\psi}_n^{(2)*}), \end{cases} \tag{2·4}$$

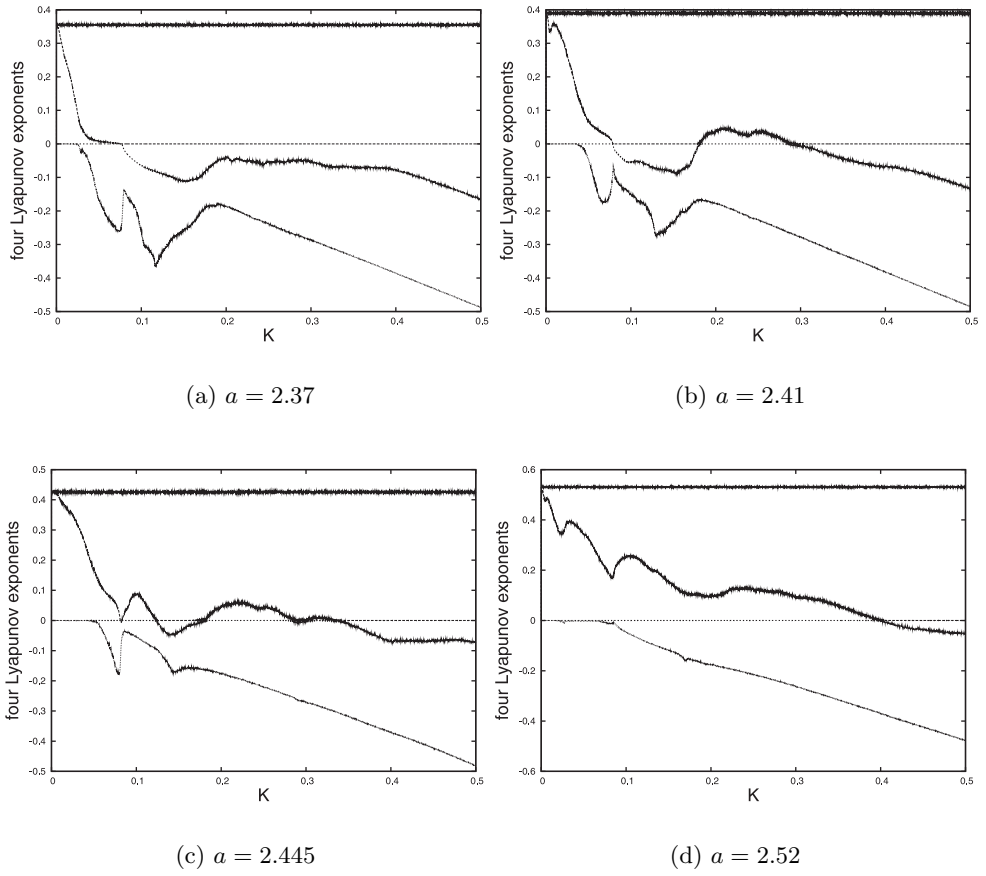


(a) $a = 2.37$ (b) $a = 2.41$

(c) $a = 2.445$ (d) $a = 2.52$

Fig. 2. Four Lyapunov exponents plotted against the coupling strength $K$ for $a = 2.37$ in (a), 2.41 in (b), 2.445 in (c), and 2.52 in (d), in which one of the two exponents originating from the chaotic driving system is always positive, and the other is always zero.

where $\bar{\psi}_n^{(j)}$ denotes $\psi_n^{(j)*}$ and $A(\Delta\omega)^* = A(-\Delta\omega)$ is used. Equation (2·4) coincides with Eq. (2·3) under the substitution $\Delta\omega \to -\Delta\omega$. Thus, the essential parameters of the system are $a_1 = a_2 = a$, $K$, and $|\Delta\omega|$.

2.1.1. CPS transitions and Lyapunov spectra

The Lyapunov spectrum consists of four Lyapunov exponents. The two of those originating from the chaotic driving system are independent of the coupling strength $K$. One is zero, and the other is positive. As shown in Fig. 2, the other two Lyapunov exponents depend on the coupling strength $K$ and are not always monotonically decreasing functions of $K$.

In Fig. 3, the symbols (•) and (▲) are plotted on the $K$-$a$ plane, at which the second-largest Lyapunov exponent changes from positive to negative and from negative to positive, respectively. The CPS transition points given by Eq. (1·6) are plotted with the symbol (∗) together with a dotted line in the $a$-$K$ plane in

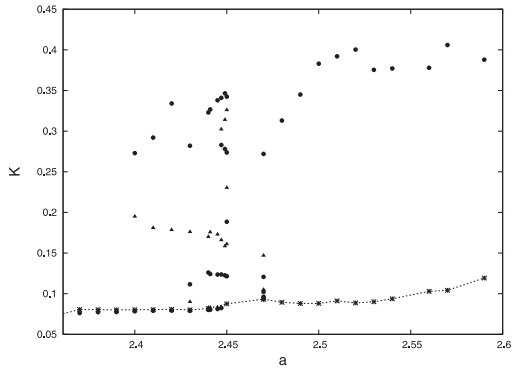


Fig. 3. The symbols (•) and (▲) are plotted on the $K$-$a$ plane, at which the second-largest Lyapunov exponent changes from positive to negative and from negative to positive, respectively, as the coupling strength $K$ is increased for the unidirectional coupling. The CPS transition points given by Eq. (1·6) are plotted with the symbol (∗) together with a dotted line in the $a$-$K$ plane.

Fig. 3. For $a \lesssim 2.45$ with the smaller positive largest Lyapunov exponent, the CPS transition point (×) almost coincides with the GS transition point (•). For $2.4 \lesssim a \lesssim 2.44$, two positive Lyapunov exponents exist between the upper symbol (•) and the lower symbol (▲) yielding hyperchaos, and a single positive Lyapunov exponent exists immediately after the CPS is achieved. For $a \gtrsim 2.473$ with the larger positive largest Lyapunov exponent, the coupling strength $K$ is much smaller on the CPS transition point (×) than on the GS transition point (•) with two positive Lyapunov exponents, where the second-largest Lyapunov exponent monotonically decreases with increasing $K$.

For the unidirectional coupling, GS occurs when one of the positive Lyapunov exponents becomes negative. To confirm the condition under which GS occurs, it is also verified that $4 \times 10^6$ replicas of the response system with arbitrarily chosen different initial states collapse in the long run.

2.1.2. Return maps

We consider RMs $\Delta\theta_{n+n_0} = R_{n_0}(\Delta\theta_n)$ of the phase difference $\Delta\theta_n$, where $n_0$ is a suitable time difference. Just before the CPS is achieved, the phase difference $\Delta\theta_n$ has a similar mechanism of Type I intermittency owing to the tangent bifurcation, which consists of a laminar part near the diagonal and a reinjection part corresponding to the phase slip, as shown in Fig. 4. Immediately after the CPS is achieved, the phase is locked in a finite range.[17)]

We plot the RMs of the phase difference $\Delta\theta_n$ in Fig. 5, where RMs of the phase difference $\Delta\theta$ for the unidirectional coupling ($\Delta\theta_n$, $\Delta\theta_{n+n_0}$) are plotted. The left-hand side is given for $a = 2.37$ and $n_0 = 10$ with a single positive Lyapunov exponent, and the right-hand side for $a = 2.52$ and $n_0 = 10$ with two positive Lyapunov exponents. The coupling strength $K$ is chosen where the CPS is slightly broken in (a) ($K = 0.079$ (left) and $K = 0.089$ (right)) and slightly achieved in (b) ($K = 0.081$ (left) and $K = 0.09$ (right)). The whole RM of the former has a reinjection branch as shown in Fig. 4. The corresponding trajectory fluctuates

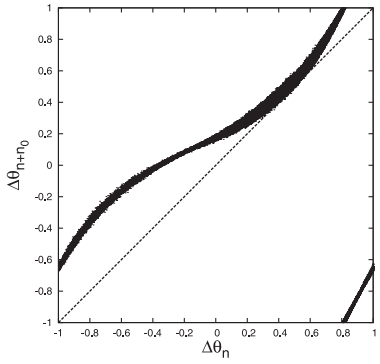


Fig. 4. RM of the phase difference $(\Delta\theta_n, \Delta\theta_{n+n_0})$ for $a = 2.52$, $K = 0.07$, and $n_0 = 10$, immediately before the CPS is achieved.

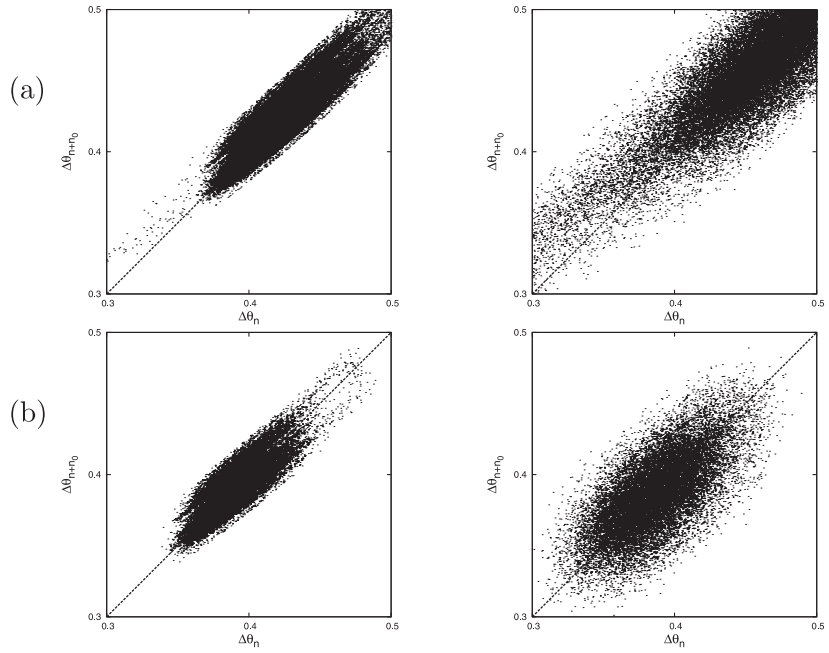


Fig. 5. RMs of the phase difference $\Delta\theta$ for the unidirectional coupling $(\Delta\theta_n, \Delta\theta_{n+n_0})$. Left ($a = 2.37$ and $n_0 = 10$ with a single positive Lyapunov exponent) and right ($a = 2.52$ and $n_0 = 10$ with two positive Lyapunov exponents). The coupling strength $K$ is chosen, where the CPS is slightly broken in (a) ($K = 0.079$ (left) and $K = 0.089$ (right)) and slightly achieved in (b) ($K = 0.081$ (left) and $K = 0.09$ (right)).

around the diagonal indicating phase locking, but eventually passes through the reinjection branch indicating unlocking. This process is repeated in an irregular manner, so that such a fluctuat-nec-mergitur trajectory is one of the characteristics of the breakdown of the CPS. We see that there are sharp edges in (a) and smooth edges in (b). The sharpness of the edges is confirmed with a probability density function of $R_{n_0}(\Delta\theta_n)$, as shown in Fig. 6.

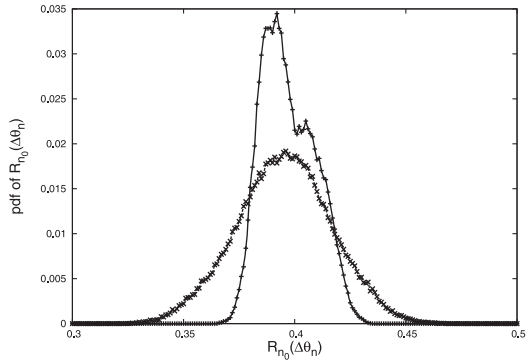


Fig. 6. Probability density functions of RMs $R_{n_0}(\Delta\theta_n)$ for $0.39 < \Delta\theta_n < 0.41$. For $(a, K) = (2.37, 0.81)$, the symbol $(+)$ is plotted, where GS is achieved, and for $(a, K) = (2.52, 0.9)$, the symbol $(*)$ is plotted, where GS is not achieved.

### 2.2. *Bidirectional coupling*

We consider here a symmetric interaction between two oscillators $\psi^{(1)}$ and $\psi^{(2)}$, where the coupling term is given by $\mathcal{D}g_{1,2} = (K/2)(g_{2,1} - g_{1,2})$ and $\hat{\Lambda}$ satisfies

$$\hat{\Lambda} = \begin{pmatrix} i\omega_1 - \frac{K}{2} & \frac{K}{2} \\ \frac{K}{2} & i\omega_2 - \frac{K}{2} \end{pmatrix}, \tag{2·5}$$

so that we have

$$\begin{cases} \psi_{n+1}^{(1)} &= J_K(\omega_1 - \omega_2)e^{i\omega_1} f_{a_1}(\psi_n^{(1)}, \psi_n^{(1)*}) + J'_K(\omega_1 - \omega_2)e^{i\omega_2} f_{a_2}(\psi_n^{(2)}, \psi_n^{(2)*}), \\ \psi_{n+1}^{(2)} &= J'_K(\omega_2 - \omega_1)e^{i\omega_1} f_{a_1}(\psi_n^{(1)}, \psi_n^{(1)*}) + J_K(\omega_2 - \omega_1)e^{i\omega_2} f_{a_2}(\psi_n^{(2)}, \psi_n^{(2)*}) \end{cases} \tag{2·6}$$

with

$$J_K(\Delta\omega) \equiv e^{-\frac{i}{2}\Delta\omega} e^{-\frac{K}{2}} \left[ \cosh \frac{\sqrt{K^2 - (\Delta\omega)^2}}{2} + i\Delta\omega \frac{\sinh \frac{\sqrt{K^2-(\Delta\omega)^2}}{2}}{\sqrt{K^2 - (\Delta\omega)^2}} \right], \tag{2·7}$$

$$J'_K(\Delta\omega) \equiv e^{\frac{i}{2}\Delta\omega} e^{-\frac{K}{2}} \frac{K \sinh \frac{\sqrt{K^2-(\Delta\omega)^2}}{2}}{\sqrt{K^2 - (\Delta\omega)^2}}, \tag{2·8}$$

which have the following symmetries : $J_k(-\Delta\omega) = J_k(\Delta\omega)^*$ and $J'_k(-\Delta\omega) = J'_k(\Delta\omega)^*$. Since the system is invariant under the transformation $\psi_n^{(j)} \to e^{i\varphi}\psi_n^{(j)}$, a vanishing Lyapunov exponent always exists.

#### 2.2.1. CPS transitions and Lyapunov spectra

The Lyapunov spectrum is plotted against the coupling strength $K$ for $a = 2.38$ in Fig. 7(a) and $a = 2.56$ in Fig. 7(b). We see that the largest and second-largest Lyapunov exponents change between positive, zero, and negative. In Fig. 8, we plot the symbols $(\bullet)$ and $(\blacktriangle)$ on the $K$-$a$ plane where the largest Lyapunov exponent changes from positive to a constant value of zero and from a constant value of zero

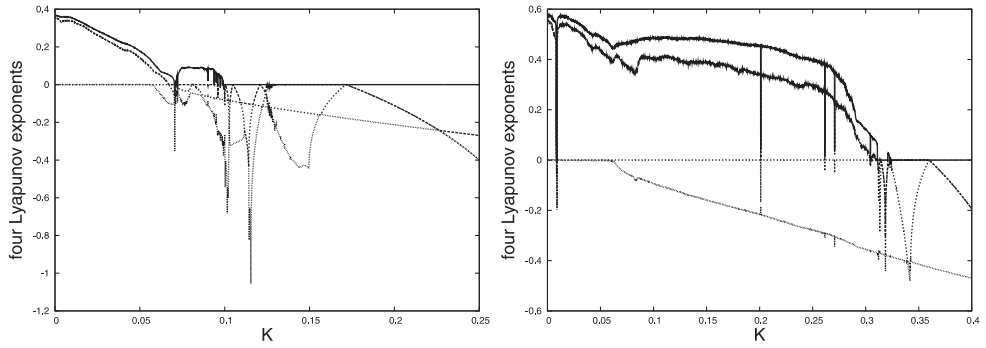


(a) $a = 2.38$ (b) $a = 2.56$

Fig. 7. Four Lyapunov exponents plotted against the coupling strength $K$ for $a = 2.38$ in (a) and $a = 2.56$ in (b).

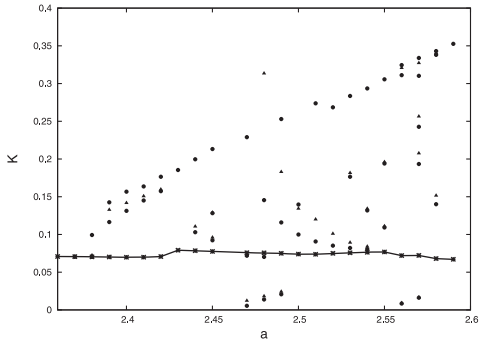


Fig. 8. The symbols (•) and (▲) are plotted on the $K$-$a$ plane where the largest Lyapunov exponent changes from positive to a constant value of zero and from a constant value of zero to positive, respectively, as the coupling strength $K$ is increased for the bidirectional coupling. The CPS transition points given by Eq. (1·6) are plotted with the symbol (∗) together with a solid line in the $a$-$K$ plane.

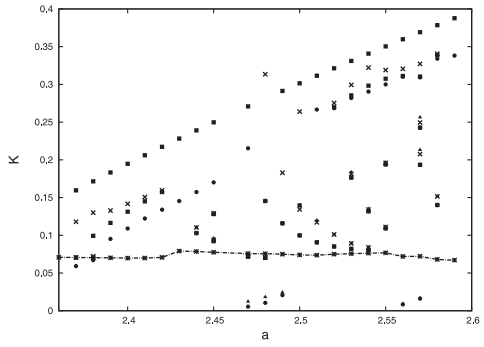


Fig. 9. The second-largest Lyapunov exponent changes from positive to zero (•), from zero to negative (■), from negative to zero (×), and from zero to positive (▲), as the coupling strength $K$ is increased for the bidirectional coupling. The CPS transition points given by Eq. (1·6) are plotted with the symbol (∗) together with a solid line in the $a$-$K$ plane.

to positive, respectively, as the coupling strength $K$ is increased. The CPS transition points given by Eq. (1·6) are plotted with the symbol (∗) together with a solid line in the $a$-$K$ plane. In Fig. 9, the second-largest Lyapunov exponent changes from positive to zero (•), from zero to negative (■), from negative to zero (×), and from zero to positive (▲), as the coupling strength $K$ is increased. The CPS transition points given by Eq. (1·6) are plotted with the symbol (∗) together with a solid line in the $a$-$K$ plane.

Note that multiple attractors and hysteresis phenomena are observed for some

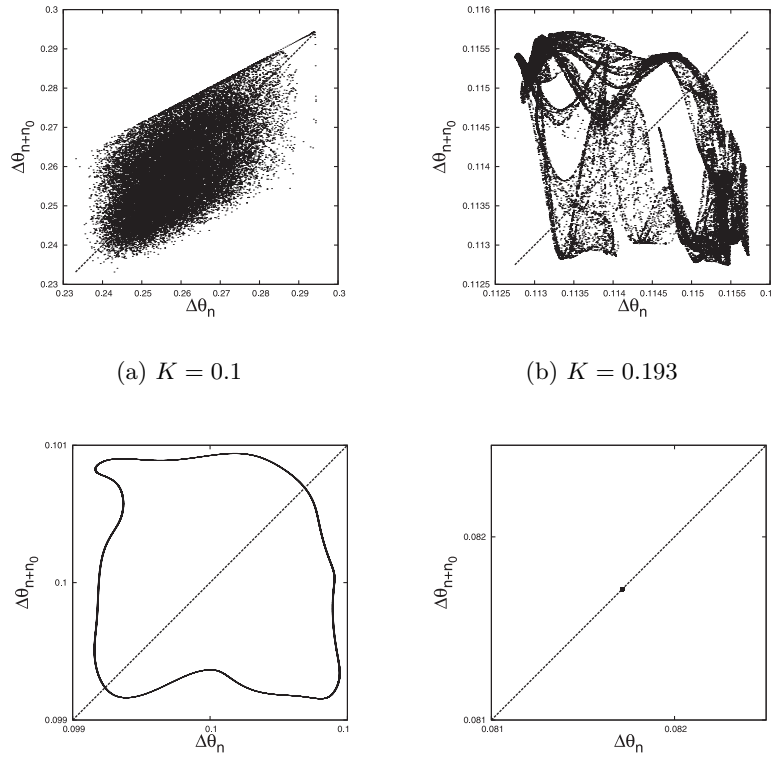


(a) $K = 0.1$ (b) $K = 0.193$

(c) $K = 0.22$ (d) $K = 0.27$

Fig. 10. RMs $(\Delta\theta_n, \Delta\theta_{n+n_0})$ for the Lyapunov spectra $(+,+,0,-)$, $(+,0,-,-)$, $(0,0,-,-)$, and $(0,-,-,-)$, respectively, for $K = 0.1$ in (a), 0.193 in (b), 0.22 in (c), and 0.27 in (d) with $a = 2.45$ for $n_0 = 10$.

regions in the $a$-$K$ plane. We fix the initial conditions as $\psi_0^{(1)} = 1 - 0.8i$ and $\psi_0^{(2)} = -0.7$ in the following.

2.2.2. Return maps

In the case of the bidirectional coupling with a sufficiently large coupling strength, no positive Lyapunov exponents exist for any $a$. As shown in Fig. 10, the RM of the phase difference $(\Delta\theta_n, \Delta\theta_{n+n_0})$ is classified into periodic points for $(0,-,-,-)$, tori for $(0,0,-,-)$, chaos for $(+,0,-,-)$, and hyperchaos for $(+,+,0,-)$.

We show the RMs $(\Delta\theta_n, \Delta\theta_{n+n_0})$ of the phase difference $\Delta\theta$ in Fig. 11, where the CPS is slightly broken in (a) ($K = 0.0702$ (left) and $K = 0.061$ (right)) and slightly achieved in (b) ($K = 0.075$ (left and right)) for $a = 2.38$ (left) and 2.56 (right) for $n_0 = 10$.

## §3. Large-deviation analysis

When the CPS is slightly broken, intermittent phase slips appear, which can be explained from the plot of $\Delta\theta_{n+n_0}$ against $\Delta\theta_n$, as shown in Fig. 4. The behavior

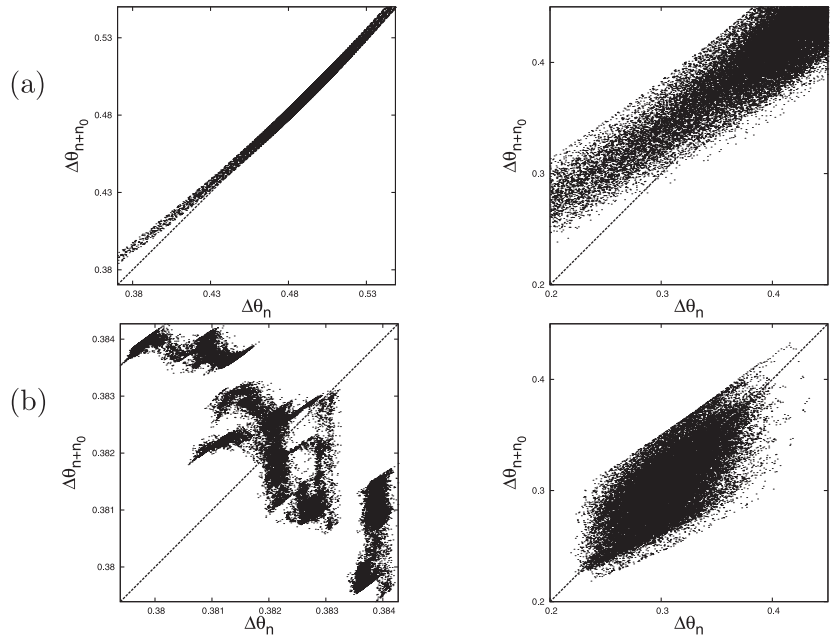


Fig. 11. RMs $(\Delta\theta_n, \Delta\theta_{n+n_0})$ of the phase difference $\Delta\theta$, where the CPS is slightly broken in (a) ($K = 0.0702$ (left) and $K = 0.061$ (right)) and slightly achieved in (b) ($K = 0.075$ (left and right)) for $a = 2.38$ (left) and 2.56 (right) for $n_0 = 10$.

of the phase slips can be characterized by the large-deviation property of the phase difference. Following the large-deviation analysis of the stationary temporal fluctuations by Fujisaka and Inoue,[18] we study the statistical properties of the phase difference in this section.

The long-time average of the phase difference is expressed as

$$\Delta\Omega = \lim_{T\to\infty} \frac{\Delta\theta_T - \Delta\theta_0}{T} = \lim_{T\to\infty} \frac{1}{T} \sum_{n=0}^{T-1} u_n, \tag{3·1}$$

where the instantaneous value of the phase difference $u_n \equiv \Delta\theta_{n+1} - \Delta\theta_n$ is introduced. For a large but finite time $T$, the finite-time average

$$\bar{u}_T \equiv \frac{1}{T} \sum_{n=0}^{T-1} u_n = \frac{\Delta\theta_T - \Delta\theta_0}{T} \tag{3·2}$$

fluctuates around the long-time average $\Delta\Omega$ and its property gives a useful characterization of the system.[8] The probability density function $P_T(u)$ of $\bar{u}_T$ is expected to obey the following scaling,

$$P_T(u) = \langle \delta(u - \bar{u}_T) \rangle \propto \exp(-TS(u)), \tag{3·3}$$

where $\langle\cdot\rangle$ denotes the long-time average, and the fluctuation spectrum $S(u)$, also known as the rate function, is obtained, for $T$ being much larger than the correlation

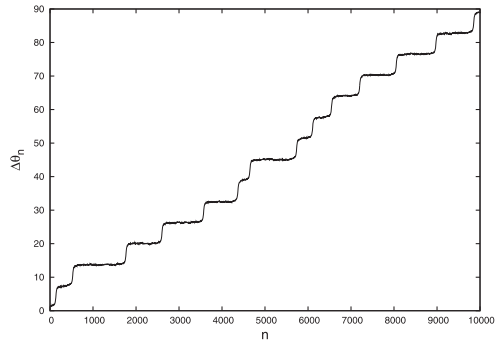


Fig. 12. Time series of the phase difference $\Delta\theta_n$ for Eq. (2·6) with $K = 0.071$ and $a = 2.51$.

decay time of $u_n$. On the basis of the statistical property of phase slips, the fluctuation spectrum is derived theoretically in Appendix A, which is compared with the numerical results in the following.

When the CPS is slightly broken, the phase difference $\Delta\theta_n$ between the two oscillators exhibits intermittent behavior similar to Type I intermittency. As shown in the RM of Fig. 4, a similar structure to tangent bifurcation exists, where $\Delta\theta_n$ stays in a *channel* around the diagonal for a long time, and passes through the channel with a characteristic time $\tau_*$ that diverges towards the CPS transition. The latter motion is called *phase slip*. These two types of motion of $\Delta\theta_n$ are clearly seen in its time series, as shown in Fig. 12.

Hereafter, we assume that the phase slip occurs in the positive direction of $\Delta\theta$ only, and time intervals between the phase slips are independent of each other. The probability distribution function $\rho(\tau)$ of the phase slip interval $\tau$ is assumed as $\rho(\tau) = \gamma \exp\big(-\gamma(\tau - \tau_*)\big)$ for $\tau \geq \tau_* > 0$ and $\rho(\tau) = 0$ otherwise, also given in Eq. (A·10), where the long-time average $\langle\tau\rangle$ and the minimum phase slip interval $\tau_*$ satisfy the relation $\langle\tau\rangle = \tau_* + \gamma^{-1}$. An exponential function form of $\rho(\tau)$ is based on the assumption that the phase slips are independent of each other and obey a Poisson process, which may be justified since $\langle\tau\rangle$ grows as $\log\langle\tau\rangle \propto \tau_*$.[9)]

Under the above assumptions, as shown in Appendix A, the fluctuation spectrum is given by

$$S(u) = \frac{1}{2\pi}\left(-u\log\Big(1 + \frac{2\pi\gamma}{\alpha}\frac{\alpha - u}{u}\Big) - \frac{2\pi\gamma}{\alpha}(u - \alpha)\right), \tag{3·4}$$

which satisfies $S(0) = \gamma$, $S(u) = \infty$ for $u < 0$ or $u > \frac{2\pi}{\tau_*}$, and $\lim_{u \to 2\pi/\tau_* - 0} S(u) = \infty$. Around the long-time average $\alpha = \langle u\rangle = \Delta\Omega$, Eq. (3·4) is expanded in the form of the central limit theorem as

$$S(u) = \frac{(u - \alpha)^2}{4D} \tag{3·5}$$

with $D = \frac{\alpha^3}{4\pi\gamma^2}$, which is the phase diffusion constant

$$D = \lim_{T \to \infty} \frac{\langle(\Delta\theta_T - \Delta\theta_0 - T\Delta\Omega)^2\rangle}{2T}. \tag{3·6}$$

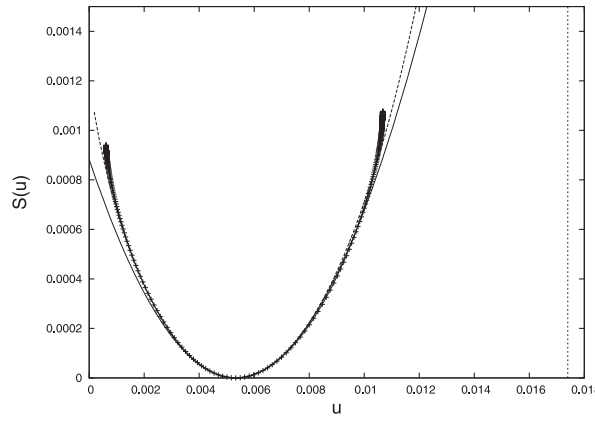


Fig. 13. Fluctuation spectrum $S(u)$ for Eq. (2·6) with $K = 0.071$ and $a = 2.51$ below the CPS transition point from the numerical result (+) and the theoretical estimation Eq. (3·4) with numerically estimated $\alpha$ and $D$ (dashed curve), whose domain is the interval between $u = 0$ and $u = \frac{2\pi}{\tau_*}$ given by Eq. (A·15). The latter is drawn with a vertical dotted line. The parabola given by the central limit theorem Eq. (3·5) is drawn as a solid curve. For the sake of comparison, the curve is extended over the domain in which the central limit theorem cannot be applied.

Thus, the parameter $\gamma$ in Eq. (3·4) is given in terms of the long-time average $\alpha$ and the phase diffusion constant $D$ as $\gamma = \alpha\sqrt{\frac{\alpha}{4\pi D}}$. We plot the fluctuation spectrum obtained from the numerically obtained distribution function of the finite-time average of the phase difference with the symbol (+) for the bidirectionally coupled system with $K = 0.071$ and $a = 2.51$ below the CPS transition point in Fig. 13, in which the theoretical estimation using Eq. (3·4) with numerically estimated $\alpha$ and $D$ is also plotted (dashed curve). The parabola given by the central limit theorem Eq. (3·5) is also drawn as a solid curve. For the sake of comparison, the curve is extended over the domain in which the central limit theorem cannot be applied. The numerical results do not reach the upper asymptote owing to the insufficient size of our statistical ensemble, but large deviations are detected clearly.

## §4. Concluding remarks

In this paper, we report on various synchronizations in discrete-time coupled chaotic rotors. For unidirectional and bidirectional couplings, we show various dynamical forms of the CPS and their relation to the Lyapunov spectra. When the control parameter $a$ is small for unidirectional coupling, the coupling strength $K$ at which CPS is achieved almost coincides with the coupling strength at which GS is achieved. On the other hand, for large $a$, the coupling strength is much smaller on the CPS transition point than on the GS transition point. The dependence of the largest Lyapunov exponent on the parameter $a$ for our chaotic map given by Eqs. (1·1) – (1·3) is very complex owing to the self-similar window structure shown in Fig. 1. However, the rough dependence given by an upper envelope of the exact dependence is a monotonically increasing function of $a$, which is similar to the logistic

map. One may choose the value of $a$ in the vicinity of the Feigenbaum point, the onset of chaos, where chaos is not developed and the largest Lyapunov exponent is small and positive. Or one may choose the value of $a$ at which chaos is fully developed. For a continuous-time system such as the Rössler system, the rough parameter dependence of the largest Lyapunov exponent is not simple in general. On the plane spanned by the parameter $a$ and the coupling strength $K$, the relative relationship between the position of the CPS transition point and the position at which either of the four Lyapunov exponents changes its sign is divided roughly into two types for the unidirectional coupling. One is the left half of Fig. 3 corresponding to the region between the Feigenbaum point and the leftmost of the period-three window shown in Fig. 1, where the chaotic attractor consists of multiple bands and chaos is not developed. The other is the right half of Fig. 3 corresponding to the region between the three-band crisis point and the attractor-destruction point, where the chaotic attractor, ignoring minute structures, consists of a single band and chaos is developed. For the bidirectional coupling, we cannot classify the relative relationship into multiple types, as shown in Figs. 8 and 9. In our results, the $a$-axis can be regarded as the axis for the largest Lyapunov exponent. The relative relationship between the CPS transition point and the sign alternation point of all the Lyapunov exponents in association with the magnitude of the largest Lyapunov exponent is quite a novel feature. In our unidirectionally coupled case, the relationship can be classified into two types, which are distinguishable by observing whether the chaotic element is fully developed. Osipov et al. also classified a similar relative relationship into three types using the coupled Rössler system.[10] In the case of the coupled Rössler system, the parameter dependence of the largest Lyapunov exponent is not simple, and the time evolution of the phase obeys a unidirectional rotation called phase-coherent rotation or a bidirectional rotation called phase-incoherent rotation, depending on the parameter. Whether the time evolution is phase-coherent is crucial in the classification into three types. In our case, it is always phase-coherent and no classification is obtained for the bidirectional coupling. It is thus impossible to compare our results simply with those obtained by Osipov et al.[10]

We study the statistical properties of the phase difference analytically and numerically by large-deviation analysis. On the basis of the grand canonical formalism, we derive the fluctuation spectrum theoretically, which is compared with the numerical results. The numerical results agree with the theoretical result, and large deviations are detected out of the domain in which the central limit theorem is applicable. Provided the RM takes the form of a noisy saddle-node bifurcation, as shown in Fig. 4, our assumption about phase-slip intervals is always satisfied, so that the large-deviation property of the phase slip is universal in this sense. In contrast, the relationship between the CPS transition points and the Lyapunov spectra depends strongly on both individual chaotic elements and the manner of coupling.

## Acknowledgements

This work was supported by a Grant-in-Aid for Scientific Research (c) (No. 20540376). We thank H. Hata, K. Ouchi, and H. Suetani for illuminating discussions.

## Appendix A
*—— Derivation of Eq. (3·4) ——*

For a real parameter $q$, we define the following generating function $M_q(n)$:

$$M_q(n) \equiv \left\langle e^{qn\bar{u}_n} \right\rangle = \int_{-\infty}^{\infty} P_n(u) e^{qnu} du. \tag{A·1}$$

For large $n$, the following scaling holds:

$$M_q(n) \propto \exp\{n\phi(q)\}, \tag{A·2}$$

where the characteristic function $\phi(q)$ is introduced in the limit of $n \to \infty$. Substituting Eq. (3·3) into Eq. (A·1), we have

$$M_q(n) \propto \int_{-\infty}^{\infty} e^{-[S(u')-qu']n} du' \tag{A·3}$$

for large $n$. Assuming the convexity of $S(u)$ ($S''(u) > 0$), we can apply the saddle-point method to the integral and we have $\phi(q)$ as the Legendre transformation of $S(u)$:

$$\phi(q) = -\min_u [S(u) - qu], \tag{A·4}$$

which has the inverse transformation

$$S(u) = -\min_q [\phi(q) - qu]. \tag{A·5}$$

Furthermore, we introduce the grand generating function $\Xi_q(\lambda)$ as

$$\Xi_q(\lambda) = \sum_{n=0}^{\infty} e^{-\lambda n} M_q(n) \sim \sum_{n=0}^{\infty} e^{(\phi(q)-\lambda)n}, \tag{A·6}$$

where the asymptotic form Eq. (A·3) is used. For $\lambda \leq \phi(q)$, we have $\Xi_q(\lambda) = \infty$, and for $\lambda > \phi(q)$, we have $\Xi_q < \infty$, so that the characteristic function $\phi(q)$ and $S(u)$ are obtained from the grand generating function $\Xi_q$.

Let $t_m$ be the time when the $m$th phase slip occurs. For the time $n$ satisfying $t_m \leq n < t_{m+1}$, we have $\sum_{i=0}^{n-1} u_i \sim 2\pi m$. For $\lambda \neq 0$, the grand partition function is rewritten as

$$\begin{aligned}
\Xi_q(\lambda) &= \sum_{n=0}^{\infty} e^{-\lambda n} M_q(n) = \left\langle \sum_{n=0}^{\infty} e^{-\lambda n} e^{q \sum_{i=0}^{n-1} u_i} \right\rangle \\
&= \left\langle \sum_{m=0}^{\infty} \sum_{k=0}^{\tau_m - 1} e^{-\lambda(\tau_0 + \cdots + \tau_{m-1} + k)} e^{2\pi m q} \right\rangle \\
&= \sum_{m=0}^{\infty} e^{2\pi m q} \left\langle e^{-\lambda(\tau_0 + \cdots + \tau_{m-1})} \frac{1 - e^{-\lambda \tau_m}}{1 - e^{-\lambda}} \right\rangle,
\end{aligned} \tag{A·7}$$

where the phase slip interval $\tau_i \equiv t_{i+1} - t_i$ is defined. With the assumption that $\tau_i$ and $\tau_j$ $(i \neq j)$ are independent of each other, we have

$$\Xi_q(\lambda) = \sum_{m=0}^{\infty} e^{2\pi m q} \left\langle e^{-\lambda \tau_i} \right\rangle^m \frac{1 - \langle e^{-\lambda \tau_m} \rangle}{1 - e^{-\lambda}}. \tag{A·8}$$

Hence, the condition

$$e^{q2\pi} \langle e^{-\lambda \tau_i} \rangle = 1 \tag{A·9}$$

yields $\lambda = \phi(q)$. Note that, for $q = 0$, Eq. (A·9) gives $\lambda = \phi(0) = 0$, which results Eq. (A·3).

When we hereby assume the probability density function of the phase slip interval $\tau$ as

$$\rho(\tau) = \begin{cases} \gamma e^{-\gamma(\tau - \tau_*)} & (\tau \geq \tau_*), \\ 0 & \text{otherwise}, \end{cases} \tag{A·10}$$

we have $\langle \tau \rangle = \tau_* + \gamma^{-1}$ and

$$\langle e^{-\lambda \tau_i} \rangle = \int_{\tau_*}^{\infty} \gamma e^{-\gamma(\tau - \tau_*)} e^{-\lambda \tau} d\tau = \frac{\gamma e^{-\lambda \tau_*}}{\gamma + \lambda}, \tag{A·11}$$

so that Eq. (A·9) and $\lambda = \phi(q)$ yield

$$\gamma e^{-\phi(q)\tau_*} = e^{-q2\pi} [\gamma + \phi(q)]. \tag{A·12}$$

We thus have the following asymptotic behaviors:

$$\begin{cases} \phi \to -\gamma, & (q \to -\infty) \\ \phi = 0, & (q = 0) \\ \phi \to \infty. & (q \to \infty) \end{cases} \tag{A·13}$$

Differentiating Eq. (A·12) with respect to $q$, we have

$$u(q) \equiv \frac{d\phi(q)}{dq} = \frac{2\pi(\gamma + \phi(q))}{1 + \gamma e^{-\phi(q)\tau_* + q2\pi} \tau_*} = \frac{2\pi}{\tau_*} \left( 1 - \frac{1}{1 + \tau_*(\gamma + \phi(q))} \right), \tag{A·14}$$

which leads to the asymptotic behaviors

$$\begin{cases} u \to 0, & (q \to -\infty, \quad \phi \to -\gamma) \\ u = \frac{2\pi}{\langle \tau \rangle}, & (q = 0, \quad \phi = 0) \\ u \to \frac{2\pi}{\tau_*}. & (q = \infty, \quad \phi = \infty) \end{cases} \tag{A·15}$$

Let us rewrite Eq. (A·12) as

$$q = \frac{1}{2\pi} \left( \phi(q)\tau_* + \log(1 + \gamma^{-1}\phi(q)) \right). \tag{A·16}$$

From this relation and the Legendre transform Eq. (A·5), we see that the fluctuation spectrum $S(u(q))$ as a function of $q$ satisfies

$$S(u(q)) = q\frac{d\phi(q)}{dq} - \phi(q) = \frac{(\gamma+\phi(q))\log(1+\gamma^{-1}\phi(q)) - \phi(q)}{1+\tau_*(\gamma+\phi(q))}, \tag{A·17}$$

which leads to the asymptotic behaviors

$$\begin{cases} S \to \gamma, & (q \to -\infty, \quad \phi \to -\gamma) \\ S = 0, & (q = 0, \quad \phi = 0) \\ S \to \infty. & (q = \infty, \quad \phi = \infty) \end{cases} \tag{A·18}$$

Equation (A·14) is rewritten as

$$\gamma + \phi(q) = \frac{1}{\tau_*}\left(\frac{1}{\frac{-\tau_* u}{2\pi}+1} - 1\right) = \frac{u}{2\pi - \tau_* u}, \tag{A·19}$$

so that Eq. (A·17) and the relation $1+\tau_*(\gamma+\phi(q)) = \frac{2\pi}{2\pi-\tau_* u}$ yield

$$\begin{aligned} S(u) &= \frac{u}{2\pi}\log\Big(\frac{u}{\gamma(2\pi-\tau_* u)}\Big) - \frac{u-\gamma(2\pi-\tau_* u)}{2\pi} \\ &= \frac{u}{2\pi}\left(\log\Big(\frac{u}{\gamma(2\pi-\tau_* u)}\Big) - (1+\gamma\tau_*)\right) + \gamma. \end{aligned} \tag{A·20}$$

Substitution of the relation $\tau_* = \langle\tau\rangle - \gamma^{-1}$ with $\alpha \equiv \langle u\rangle = 2\pi/\langle\tau\rangle$ into Eq. (A·20) yields Eq. (3·4).

## References


1) A. Pikovsky, M. Rosenblum and J. Kurths, *Synchronization: A universal concept in nonlinear sciences* (Cambridge University Press, Cambridge, 2001).
2) H. Suetani and T. Horita, Phys. Rev. E **60** (1999), 422.
3) T. Horita and H. Suetani, Phys. Rev. E **65** (2002), 056217.
4) H. Hata and S. Miyazaki, Phys. Rev. E **55** (1997), 5311.
5) S. Miyazaki and H. Hata, Phys. Rev. E **58** (1998), 7172.
6) H. Fujisaka and T. Yamada, Prog. Theor. Phys. **69** (1983), 32.
7) T. Yamada and H. Fujisaka, Prog. Theor. Phys. **70** (1983), 1240.
8) M. G. Rosenblum, A. S. Pikovsky and J. Kurths, Phys. Rev. Lett. **76** (1996), 1804.
9) S. Boccaletti, J. Kurths, G. Osipov, D. L. Valladares and C. S. Zhou, Phys. Rep. **366** (2002), 1.
10) G. V. Osipov, B. Hu, C. Zhou, M. V. Ivanchenko and J. Kurths, Phys. Rev. Lett. **91** (2003), 024101.
11) A. Politi, F. Ginelli, S. Yanchuk and Y. Maistrenko, Physica D **224** (2006), 90.
12) A. E. Hramov, A. A. Koronovskii and M. K. Kurovskaya, Phys. Rev. E **78** (2008), 036212.
13) N. F. Rulkov, M. M. Sushchik, L. S. Tsimring and H. D. I. Abarbanel, Phys. Rev. E **51** (1995), 980.
14) K. Pyragas, Phys. Rev. E **54** (1996), R4508.
15) H. Fujisaka, S. Uchiyama and T. Horita, Prog. Theor. Phys. **114** (2005), 289.
16) K. Ikeda, Opt. Commun. **30** (1979), 257.
17) N. Tsukamoto and H. Fujisaka, Physica D **233** (2007), 32.
18) H. Fujisaka and M. Inoue, Prog. Theor. Phys. **77** (1987), 1334.